Euro. Jnl of Applied Mathematics (1999), *vol.* 10, *pp.* 157–184. Printed in the United Kingdom

© 1999 Cambridge University Press

Modulated two-dimensional patterns in reaction–diffusion systems

R. KUSKE[1] and P. MILEWSKI[2]

[1] *School of Mathematics, University of Minnesota, Minneapolis, MN, USA*
(*email: rachel@math.umn.edu*)
[2] *Department of Mathematics, University of Wisconsin, Madison, WI, USA*
(*email: milewski@math.wisc.edu*)

(*Received 23 June 1997; revised 26 May 1998*)

New modulation equations for hexagonal patterns in reaction–diffusion systems are derived for parameter régimes corresponding to the onset of patterns. These systems include additional nonlinearities which are not present in Rayleigh–Bénard convection or Swift–Hohenberg type models. The dynamics of hexagonal and roll patterns are studied using a combination of analytical and computational approaches which exploit the hexagonal structure of the modulation equations. The investigation demonstrates instabilities and new phenomena not found in other systems, and is applied to patterns of flame fronts in a certain model of burner stabilized flames.

1 Introduction

Instabilities in many physical or chemical systems often lead to spatio-temporal patterns. Typical systems in which these patterns occur include convection [1, 2], chemical reactions [3–5], and nonlinear optics [6]. These patterns usually occur as the superposition of periodic waves of some component of the system, such as temperature or concentration. Borrowing the terminology from convection studies, a single such wave is usually called a roll. Near the onset of instabilities, the dynamics of the periodic waves are well described by amplitude equations for their envelopes. These amplitude equations are used to study the modulations and instabilities of the patterns. Also, the computation of pattern dynamics is often more straightforward using modulation equations rather than the full system, as, for example, in the study of patterns on a reaction front in Kuske & Matkowsky [7]. Perfect hexagonal patterns appear as the superposition of three roll solutions with wave vectors at 120°. Modulation equations for hexagonal patterns in general reaction–diffusion models typically include additional nonlinear terms, which describe instabilities and new phenomena not studied in Rayleigh–Bénard convection models [8] or Swift–Hohenberg type models [9]. In this paper we derive new evolution equations for modulated hexagonal patterns in general reaction–diffusion systems. These equations are written in a form in which the hexagonal symmetries are apparent, i.e. the new coordinates are X_1, X_2 and X_3,

$$X_1 = X, \quad X_2 = -\frac{1}{2}X + \frac{\sqrt{3}}{2}Y, \quad X_3 = -\frac{1}{2}X - \frac{\sqrt{3}}{2}Y, \tag{1.1}$$

https://doi.org/10.1017/S095679259800360X Published online by Cambridge University Press

where $(X, Y) = \epsilon^{-1}(x, y)$ are the usual two-dimensional Cartesian coordinates. Then the coupled evolution equations for the amplitudes $A_j(X_1, X_2, X_3)$, $j = 1, 2, 3$ of the three rolls are

$$\begin{aligned} A_{j_\tau} = aA_j + c\overline{A}_k\overline{A}_l + dA_{j_{\eta_j\eta_j}} + bA_j|A_j|^2 + fA_j(|A_k|^2 + |A_l|^2) \\ +ih_1(\overline{A}_k\overline{A}_l)_{\eta_j} + ih_2[(\overline{A}_k)_{\eta_k}\overline{A}_l + (\overline{A}_l)_{\eta_l}\overline{A}_k], \end{aligned} \tag{1.2}$$

for permutations of $j, k, l = 1, 2, 3$. The subscripts η_j for $j = 1, 2, 3$ denote differentiation along the direction X_j, i.e. in the direction of the wave vector for roll j,

$$\frac{\partial}{\partial \eta_j} = \frac{\partial}{\partial X_j} - \frac{1}{2}\frac{\partial}{\partial X_k} - \frac{1}{2}\frac{\partial}{\partial X_l}. \tag{1.3}$$

For some of the phenomena studied, we will also consider modulations to roll j in the direction orthogonal to X_j (that is, modulations along the roll). For this, we introduce the derivatives in the direction ξ_j, orthogonal to η_j with

$$\frac{\partial}{\partial \xi_j} = \frac{\sqrt{3}}{2}\left(\frac{\partial}{\partial X_k} - \frac{\partial}{\partial X_l}\right). \tag{1.4}$$

Including those modulations, equation (1.2) become

$$\begin{aligned} A_{j_\tau} = aA_j + c\overline{A}_k\overline{A}_l + d\left(\partial_{\eta_j} + \frac{\epsilon}{2ik_c}\partial^2_{\xi_j}\right)^2 A_j + bA_j|A_j|^2 + fA_j(|A_k|^2 + |A_l|^2) \\ +ih_1(\overline{A}_k\overline{A}_l)_{\eta_j} + ih_2[(\overline{A}_k)_{\eta_k}\overline{A}_l + (\overline{A}_l)_{\eta_l}\overline{A}_k]. \end{aligned} \tag{1.5}$$

The difference between these modulation equations and those studied by Hoyle [9] and Suschik & Tsimring [10] are the terms with coefficients h_1, h_2, referred to as non-gradient terms [2] or non-potential terms, as discussed further at the end of §2 and in Gunaratne *et al.* [11], Golovin *et al.* [12] and Echebarria [13]. We employ a combination of analytical and computational approaches which exploit the hexagonal structure of the modulation equations to determine the stability and dynamics of patterns. We use a pseudo–spectral numerical algorithm on a hexagonal grid that allows the removal of unwanted boundary effects that arise from a rectangular mesh, as used in Suschik & Tsimring [10].

The analysis and computations demonstrate the stability differences between a general reaction diffusion system and previously studied evolution equations for certain convection problems [2, 9, 10]. In the reaction–diffusion systems we consider, there are additional instabilities of both roll and perfect hexagons, which are also observed in Marangoni convection [12–14]. There are also other stable modulated two dimensional patterns which are a combination of rolls and hexagons, sometimes referred to as general hexagonal patterns. The computational results validate and complement the stability criteria obtained analytically.

In the linear stability analysis we perturb the three rolls forming the hexagonal pattern with the same small wave number. We call such perturbations 'symmetric', in contrast to the more general 'asymmetric' case of different wave number perturbations for each roll. Although such asymmetric perturbations are analytically less tractable, we observe numerically that in the case of $h_1 \neq 0$ and $h_2 \neq 0$, they lead to observable instabilities. These instabilities are important since they may occur in parameter ranges where the pattern is stable to symmetric perturbations. The application of these methods is demonstrated

https://doi.org/10.1017/S095679259800360X Published online by Cambridge University Press

for a general reaction–diffusion system and in the specific problem of a burner-stabilized flame front [7] which has the important features of the general system.

2 Modulation equations

We consider the general reaction–diffusion system, as motivated by various models [4, 15, 16]:

$$\frac{\partial \tilde{u}}{\partial t} = D\left(\frac{\partial^2 \tilde{u}}{\partial x^2} + \frac{\partial^2 \tilde{u}}{\partial y^2}\right) + f(\tilde{u};\lambda), \qquad t > 0, \quad -\infty < x, y < \infty, \tag{2.1}$$

$$\tilde{u} \text{ bounded as } x, y \to \pm\infty,$$

where t and x, y are the temporal and spatial variables, respectively, and $\tilde{u}(x, y, t; \lambda)$ and $f(\tilde{u};\lambda)$ are vector functions

$$\tilde{u} = (\tilde{u}_1, \tilde{u}_2, \ldots, \tilde{u}_m), \quad f(\tilde{u};\lambda) = (f_1, f_2, \ldots, f_m). \tag{2.2}$$

The matrix D is diagonal with non-negative elements on the diagonal. The parameter λ is real. We assume that $m \geqslant 2$. We assume that $f(\mathbf{0}) = \mathbf{0}$, so that there is a basic uniform state of $\tilde{u} = 0$. Then one can consider a perturbation $\tilde{u} = u \neq 0$ to this basic state, such as the deviation from a chemical reaction in which the species are kept constant and uniform in space and time, as in the Brusselator model [16]. In the study of a pattern on a reaction front, one can consider u as the deviation from a planar front [7].

The parameter λ is a control parameter; for values of λ above a critical value λ_c, the basic state $\tilde{u} \equiv 0$ loses stability to a periodic solution. To determine conditions for the instability of the basic solution and the types of solutions which appear as a result of the instability, we linearize (2.1) about the basic state, that is, for the perturbation $u \ll 1$. This yields

$$\frac{\partial u}{\partial t} = D\left(\frac{\partial^2 u}{\partial x^2} + \frac{\partial^2 u}{\partial y^2}\right) + \alpha_\lambda u, \tag{2.3}$$

where α_λ is the Jacobian matrix such that

$$\alpha_\lambda u \equiv \left(\frac{\partial f_i(\tilde{u};\lambda)}{\partial \tilde{u}^j}\bigg|_{\tilde{u}=\mathbf{0}}\right) u^j, \quad (i = 1, \ldots, m), \tag{2.4}$$

where superscripts indicate components of the vector u, and repeated superscripts indicate summation over $j = 1, \ldots, m$. We substitute

$$u = e^{\mu t + ik_1 x + ik_2 y} v, \quad k_1^2 + k_2^2 \equiv |k|^2, \tag{2.5}$$

into equation (2.3) to obtain

$$-|k|^2 D v + \alpha_\lambda v = \mu v. \tag{2.6}$$

Here (k_1, k_2) and μ are the wave vector and growth rate, respectively, of the perturbation u. Equation (2.6) is an eigenvalue problem for the growth rate $\mu(k_1, k_2, \lambda)$, with corresponding eigenvector v_μ. Without loss of generality, we assume that the critical value is $\lambda_c = 0$, and that the following conditions hold for μ:

(1) For $\lambda < 0$ all eigenvalues μ have negative real parts.

https://doi.org/10.1017/S095679259800360X Published online by Cambridge University Press

(2) For $\lambda = 0$ and $|k| = k_c \neq 0$, there exists an eigenvalue $\mu = 0$, and all other eigenvalues μ have negative real parts.

(3) For a range of $\lambda > 0$ there is a range of wave numbers $k_- < |k| < k_+$ such that for each $|k|$ in this range there exist an eigenvalue $\mu(k_1, k_2, \lambda) > 0$ and $\mu < 0$ for $|k|$ outside that range. In addition, the real parts of all other eigenvalues are negative.

These assumptions indicate that the basic solution, which is stable for $\lambda < 0$, loses its stability when λ passes through the critical value $\lambda_c = 0$ via a steady bifurcation. There exists a continuous band of wave numbers of perturbations for the instability region $\lambda > 0$. The curves $k_\pm$ form the neutral stability curve which has a minimum at $|k| = k_c$, which corresponds to the first unstable mode as λ is increased above λ_c. In the following analysis we consider systems near critical, that is $\lambda - \lambda_c = O(\epsilon^p)$ where $\epsilon \ll 1$, $p > 0$. In studying the patterns in this regime, one can consider any superposition of modes as a solution for u. We are interested in patterns for which the interaction between the modes are strongest, the simplest of these being hexagonal patterns. Evolution equations for the slowly varying modulations or rolls have been used to study the stability of two-dimensional patterns and the propagation of defects in patterns in convection [2] and in reaction diffusion kinetics [3]. Here, we derive these amplitude equations for the general setting of equation (2.1). At the end of this section, we compare the form of these amplitude equations with related work.

Near criticality ($\lambda \ll 1$), we define a small parameter $\epsilon \ll 1$ and set

$$\lambda = \epsilon^2 \lambda_2 + \dots. \tag{2.7}$$

Also, the solution u is small and we expand it as

$$u \sim \epsilon u_1 + \epsilon^2 u_2 + \epsilon^3 u_3 + \dots. \tag{2.8}$$

We consider the interaction of three modes, by writing

$$u_1 = R_1 e_1 v_0 + R_2 e_2 v_0 + R_3 e_3 v_0 + \text{ complex conjugates}, \tag{2.9}$$

where v_0 is the eigenvector in equation (2.6). The wave vectors of the modes e_j are separated by angles of $\pi/3$, so that

$$e_1 = e^{ik_c x}, \quad e_2 = e^{ik_c(-x/2+\sqrt{3}y/2)}, \quad e_3 = e^{ik_c(-x/2-\sqrt{3}y/2)}. \tag{2.10}$$

We assume the amplitudes R_j are slowly varying in space and time, so that $R_j = R_j(X, Y, T, \tau)$, where

$$X = \epsilon x, \quad Y = \epsilon y, \quad T = \epsilon t, \quad \tau = \epsilon^2 t. \tag{2.11}$$

Typically only one slow time scale is introduced in convection or Swift–Hohenberg-type models. Here the introduction of two time scales is necessary for the systematic derivation of the amplitude equations, as seen below.

We expand the nonlinear function $f(\tilde{u}; \lambda)$ about the basic solution $\tilde{u} = 0$, i.e. for small perturbations u

$$f(\tilde{u}; \lambda) \sim \alpha_\lambda u + \beta_\lambda(u, u) + \gamma_\lambda(u, u, u) + \delta_\lambda(u, u, u, u) + \dots, \tag{2.12}$$

https://doi.org/10.1017/S095679259800360X Published online by Cambridge University Press

where $\alpha_\lambda u$ is defined in equation (2.4) and

$$\beta_\lambda(u,u) \equiv \frac{1}{2!}\left\{\left.\frac{\partial^2 f_i(\tilde{u};\lambda)}{\partial\tilde{u}^j\partial\tilde{u}^k}\right|_{\tilde{u}=\mathbf{0}} u^j u^k\right\}, \tag{2.13}$$

$$\gamma_\lambda(u,u,u) \equiv \frac{1}{3!}\left\{\left.\frac{\partial^3 f_i(\tilde{u};\lambda)}{\partial\tilde{u}^j\partial\tilde{u}^k\partial\tilde{u}^l}\right|_{\tilde{u}=\mathbf{0}} u^j u^k u^l\right\}, \tag{2.14}$$

where repeated superscripts indicate summation. Since α_λ, β_λ and γ_λ are in general functions of λ, we expand as

$$\alpha_\lambda \sim \alpha_0 + \lambda\alpha_1 + \ldots, \tag{2.15}$$

where $\alpha_0 = \alpha_\lambda|_{\lambda=0}$,

$$\alpha_1 = \left.\frac{\partial\alpha_\lambda}{\partial\lambda}\right|_{\lambda=0}, \tag{2.16}$$

and similarly for β and γ. Substituting equations (2.7), (2.8), (2.12) and (2.15) into equation (2.1), and collecting the coefficients of like powers of ϵ yields

$$\begin{aligned} O(\epsilon) &: L_0 u_1 \equiv \left[\frac{\partial}{\partial t} - D\left(\frac{\partial^2}{\partial x^2} + \frac{\partial^2}{\partial y^2}\right) - \alpha_0\right] u_1 = 0, \\ O(\epsilon^j) &: L_0 u_j = r_j. \qquad j = 2,3,\ldots, \end{aligned} \tag{2.17}$$

where

$$\begin{aligned} r_2 &= \beta_0(u_1,u_1) + 2D\left(u_{1Xx} + u_{1Yy}\right) - u_{1T}, \\ r_3 &= \lambda_2\alpha_1 u_1 + 2\beta_0(u_1,u_2) + \gamma_0(u_1,u_1,u_1) \\ &\quad + 2D\left(u_{2Xx} + u_{2Yy}\right) + D\left(u_{1XX} + u_{1YY}\right) - u_{2T} - u_{1\tau}. \end{aligned} \tag{2.18}$$

It is possible to solve for u_j, $j = 2,3,\ldots$, if the right-hand side of the equation for u_j in equation (2.17) is orthogonal to the homogeneous solutions $(v_0^*\bar{e}_1, v_0^*\bar{e}_2, v_0^*\bar{e}_3)$ of the adjoint equation $L_0^* u = 0$. This solvability condition is applied with an appropriately defined inner product. In this case, it is

$$\int_0^{2\pi/k_1}\int_0^{2\pi/k_2} (r_j\cdot\bar{e}_l v_0^*)dy\,dx \equiv \langle r_j, \bar{e}_l v_0^*\rangle = 0, \tag{2.19}$$

where k_1, k_2 are chosen to include a period of the integrand in equation (2.19). We use the normalization $\langle e_k v_0, \bar{e}_l v_0^*\rangle = \delta_{kl}$. These solvability conditions yield equations for the slowly varying amplitudes R_j. We outline this process in some detail to illustrate a particular feature: that the appropriate terms in the amplitude equations are obtained at two different orders in the perturbation expansion. (For the sake of clarity, the reader is reminded that when k is used as a subscript it denotes indexing and not wave number.)

First, we consider the equation obtained at $O(\epsilon^2)$. Applying the solvability condition yields

$$\langle r_2, v_0^*\bar{e}_l\rangle = R_{lT} - c_0\overline{R}_m\overline{R}_n = 0, \tag{2.20}$$

with

$$c_0 = \langle\beta_0(\bar{e}_m v_0, \bar{e}_n v_0), \bar{e}_l v_0^*\rangle, \tag{2.21}$$

https://doi.org/10.1017/S095679259800360X Published online by Cambridge University Press

where $l, m, n = 1, 2, 3$ and cyclic permutations give us the three amplitude equations. Of course, these are not the full evolution equations for R_j, $j = 1, 2, 3$. As is well known from symmetry considerations (see, for example, Swift [1]) in the case when the modulations are temporal only, the correct amplitude equations include cubic terms. In the context of deriving the evolution equations from a perturbation expansion, including cubic terms corresponds to including higher order terms, that is, those obtained from the solvability conditions (2.20) and from the next order [7]. From a dynamical point of view, the cubic terms play the role of stabilizing the hexagonal pattern which bifurcates subcritically from the basic state.

This complication is not encountered in the derivation of evolution equations in the context of Rayleigh–Bénard convection. In that application, the symmetries are such that the coefficient $c_0 = 0$ in equation (2.20). If the coefficient $c_0 = 0$, then it is appropriate to consider modulations on the time scale τ only, so that $(R_j)_T = 0$. Then the solvability conditions (2.20) are automatically satisfied, and the evolution equations will be given by the solvability conditions at $O(\epsilon^3)$. This is the procedure used in Kuznetsov *et al.* [2]. In many applications $c_0 \neq 0$ [3, 7], so that the solvability condition at $O(\epsilon^2)$ is combined with the $O(\epsilon^3)$ solvability condition to obtain the correct evolution equations, as we discuss below. Regardless of the value of c_0, we determine u_2 which is used in the higher order equations. We shall do this for the case $c_0 \neq 0$, since this is the general case for reaction–diffusion equations.

The rest of the derivation is straightforward, and is outlined in Appendix A. After solving for u_2 (A 3), we substitute in r_3 and apply the solvability condition (2.19). This yields solvability conditions of the form

$$S_{jT} + R_{j\tau} = aR_j + c_0(\overline{S}_k\overline{R}_l + \overline{R}_k\overline{S}_l) + dR_{j\eta_j\eta_j} + bR_j|R_j|^2 + fR_j(|R_k|^2 + |R_l|^2)$$
$$+ih_1(\overline{R}_k\overline{R}_l)_{\eta_j} + ih_2[\overline{R}_{k\eta_k}\overline{R}_l + \overline{R}_{l\eta_l}\overline{R}_k], \tag{2.22}$$

and $j, k, l = 1, 2, 3$ with cyclic permutations to obtain the three solvability conditions.

Since R_j, $j = 1, 2, 3$ are the amplitudes corresponding to the homogeneous part of u_1 and S_j is the amplitude for the homogeneous part of u_2, we combine the solvability condition from $O(\epsilon^2)$ and $O(\epsilon^3)$ in an equation for $A_j = R_j + \epsilon S_j$ for $j = 1, 2, 3$,

$$A_{jT} + \epsilon A_{j\tau} = \epsilon aA_j + (c_0 + \epsilon c_1)\overline{A}_k\overline{A}_l + \epsilon dA_{j\eta_j\eta_j} + \epsilon bA_j|A_j|^2 + \epsilon fA_j(|A_k|^2 + |A_l|^2)$$
$$+i\epsilon h_1(\overline{A}_k\overline{A}_l)_{\eta_j} + i\epsilon h_2[(\overline{A}_k)_{\eta_k}\overline{A}_l + (\overline{A}_l)_{\eta_l}\overline{A}_k] + O(\epsilon^2). \tag{2.23}$$

Truncating at $O(\epsilon)$ and writing $c_0 + \epsilon c_1 = c, \partial_{\hat{\tau}} = \partial_T + \epsilon\partial\tau$, $\hat{b} = \epsilon b$, and similarly for a, f, d, h_1, and h_2, we obtain equation (1.2) (after dropping the hats). These equations are written in a form in which the hexagonal symmetries are apparent, using equation (1.3). These equations describe the dynamics of modulated hexagonal patterns, as discussed further in §3.1. In §3.2 we use equation (1.2) to determine the stability of rolls to hexagonal perturbations. To describe instabilities to other perturbations, such as the zigzag instability to perturbations transverse to the rolls, it is necessary to include higher order derivative terms, corresponding to modulations along the rolls. In this case, the term $dA_{j\eta_j\eta_j}$ in equation (1.2) is replaced by $d\left(\partial_{\eta_j} + (\epsilon/2ik_c)\partial^2_{\xi_j}\right)^2 A_j$ (see equation (1.5)). This is discussed further in the following section.

https://doi.org/10.1017/S095679259800360X Published online by Cambridge University Press

We comment on the fact that the terms in equation (2.23) come from $O(\epsilon^2)$ solvability conditions and the $O(\epsilon^3)$ solvability condition, so that there is a factor of ϵ in front of some of the terms. As mentioned above, the cubic terms such as $bA_j|A_j|^2$ and $fA_j(|A_k|^2+|A_l|^2)$ are crucial in describing the stability of hexagons, since these nonlinear interactions stabilize the hexagonal patterns which bifurcate subcritically from the uniform state. These terms are obtained from the solvability conditions at $O(\epsilon^3)$, that is, at the next higher order from equation (2.20). Therefore, for consistency, we include all terms obtained from the solvability conditions at that order. In the case of $c_0 \neq 0$ in equation (2.20), we obtain the terms $ih_1(\overline{A}_k\overline{A}_l)_{\eta_j}$ and $ih_2[(\overline{A}_k)_{\eta_k}\overline{A}_l+(\overline{A}_l)_{\eta_l}\overline{A}_k]$ in the amplitude equations. As shown in the following stability analysis and computations, these terms also have an effect on the stability of the patterns.

Since there is a coefficient of ϵ in the equations (2.23) we discuss how these terms may be balanced. The coefficient c_0 can take small values, so that all terms may be of the same order for certain physical parameter values. In this case, as in the case when $c_0=0$ in equation (2.20), one can set $c_0=\epsilon c$, and allow A to be a function of the slow time τ only, not of T. In general for $c_0=O(1)$, one applies the method of Bernoff *et al.* [15] to combine contributions at different orders, as shown above. In Bernoff *et al.* [15] this approach was used to study mean field effects described by evolution equations which include higher order terms. In the case when the additional higher order terms describe instabilities or stability not determined from the lower order equations, these terms must be included. This is the case in this paper, as well as in Bernoff *et al.* [15].

The main difference between equation (1.2) and the evolution equations studied by Lauxeral *et al.* [3] and Suschik & Tsimring [10] are the nonlinear terms with coefficient h_j, the non-gradient terms. Envelope equations with non-gradient terms have also been derived for Rayleigh–Bénard convection models. In the context of non-equilateral hexagonal patterns $h_1=2h_2$ [2], and in the context of non-Boussinesq effects $h_1=0$ [18]. The non-gradient terms with coefficient h_1 have been discussed by Gunaratne *et al.* [11] in the context of generalized Swift–Hohenberg models with nonlinear gradient terms. Equations of the form (1.2) for general h_1 and h_2 are obtained in the context of Marangoni convection, as shown by Golovin *et al.* [12] and references therein, and by Echebarria [13].

In the stability analysis below we consider symmetric perturbations to perfect hexagons and rolls for arbitrary coefficients in equation (1.2). Stability of these patterns to other types of perturbations and the stability of non-equilateral hexagons has been studied by Nuz *et al.* [14]. In Golvin *et al.* [12] the stability was considered for coefficients consistent with Marangoni convection. In the case when $h_1=h_2=0$, as in Lauzeral *et al.* [3] and Suschik & Tsimring [10], it is useful to consider $A_j=r_je^{i\theta_j}$. With the assumption that the amplitude evolves adiabatically with the phase it is possible to derive phase equations for θ_j describing the hexagonal patterns, thus reducing the complexity of the stability analysis [9, 10, 17]. When $h_1\neq 0$ and $h_2\neq 0$, there are additional complications in these coupled phase equations so that it is not necessarily advantageous to pursue such an approach.

3 Stability

In this section we consider the stability analysis of simple finite amplitude solutions to equation (1.2). We first consider the stability of perfect hexagons to long wave perturba-

https://doi.org/10.1017/S095679259800360X Published online by Cambridge University Press

tions, and then the stability of a single roll to general perturbations. In both cases we show that when h_1, h_2 are non-zero, there are new stability constraints. The analysis uses equation (1.2), without transformations which normalize some of the coefficients. This allows a comparison with previous analyses, such as those of Kuske & Matkowsky [7] and Suschik & Tsimring [10], to understand the effects of the additional quadratic terms.

3.1 Stability of hexagons

First, we consider the stability of symmetric hexagonal modulations,

$$A_j = r_0 e^{iqX_j}, \tag{3.1}$$

as solutions of equation (1.2). In the following we find it useful to define the quantity

$$B = c - h_1 q + 2h_2 q, \tag{3.2}$$

The stationary solutions (3.1) exist for r_0 and q satisfying

$$a + Br_0 + (b + 2f)r_0^2 = dq^2 > 0. \tag{3.3}$$

That is,

$$r_0 = \frac{-B \pm \sqrt{B^2 - 4(a - dq^2)(b + 2f)}}{2(b + 2f)}, \tag{3.4}$$

where r_0 is real for

$$dq^2 < a - \frac{B^2}{4(b + 2f)}. \tag{3.5}$$

Then one can determine the stability of such solutions for

$$A_j = (r_0 + \hat{p}_j)e^{iqX_j + i\hat{\Omega}_j}. \tag{3.6}$$

Substituting in equation (1.2) and linearizing about $\hat{p}_j = 0$ and $\hat{\Omega}_j = 0$ yields coupled linear equations for $\hat{p}_j$ and $\hat{\Omega}_j$. With the ansatz that

$$\begin{aligned} \hat{p}_j &= p_j e^{\Lambda t + i\gamma_1 X + i\gamma_2 Y}, \\ \hat{\Omega}_j &= \Omega_j e^{\Lambda t + i\gamma_1 X + i\gamma_2 Y}, \end{aligned} \tag{3.7}$$

we obtain stability conditions for the regular hexagonal patterns in terms of the eigenvalues Λ of the matrix given in Appendix B. That is, the regular hexagons are stable to small perturbations for $Re(\Lambda) < 0$. The perturbations in equation (3.7) are symmetric in the sense that the three rolls are modified by the same wave number (γ_1, γ_2). This corresponds to perturbing the hexagonal pattern as a whole with a long wave modulation.

We consider the limit of long wave perturbations, i.e. $\gamma_1 \ll 1$ and $\gamma_2 \ll 1$. To leading order ($\gamma_1 = \gamma_2 = 0$) the eigenvalues of the matrix are

$$\begin{aligned} \Lambda_{1,2} &= 0 \qquad \text{(multiplicity 2)}, \\ \Lambda_3 &= -3Br_0, \\ \Lambda_4 &= Br_0 + 2br_0^2 + 4fr_0^2, \\ \Lambda_{5,6} &= -2Br_0 + 2br_0^2 - 2fr_0^2 \qquad \text{(multiplicity 2)}. \end{aligned} \tag{3.8}$$

https://doi.org/10.1017/S095679259800360X Published online by Cambridge University Press

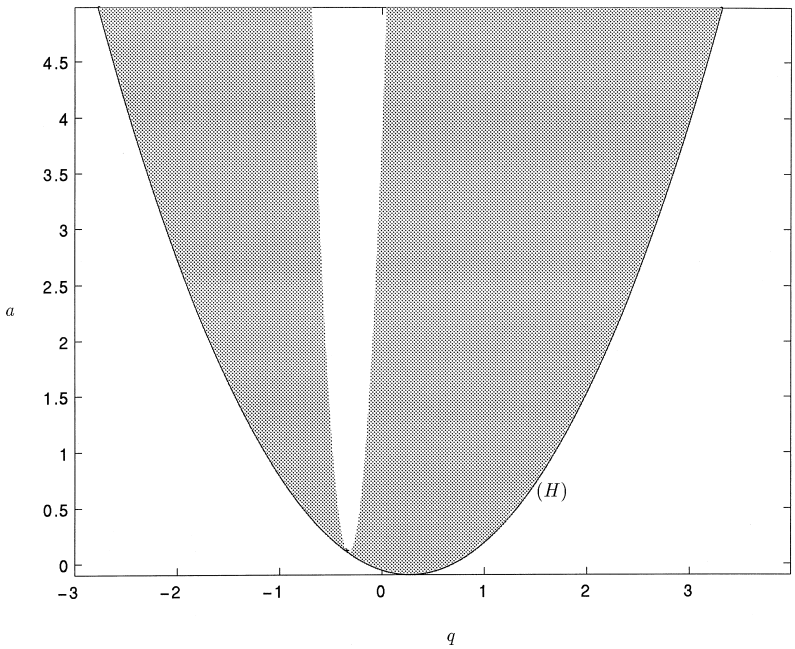


FIGURE 1. Existence and stability of perfect hexagonal patterns (3.1) for $c = d = 1$, $b = -1$, $f = -2$, $h_1 = -1$, $h_2 = 1$. Perfect hexagonal patterns exist above the curve (H). The shaded region corresponds to stability to zero mode perturbations ($\gamma_1 = \gamma_2 = 0$ in (3.7)). For these values of q and a the eigenvalues $\Lambda_j < 0$, $j = 3, 4, 5$.

For $q = h_1 = h_2 = 0$, the stability conditions are the same as those obtained for perfect hexagons in Kuske & Matkoswky [7]. The conditions $\Lambda_j < 0$, $j = 3, 4, 5$ are shown in the a–q plane in Figure 1. For the case of $h_1 \neq 0$ and $h_2 \neq 0$, when the additional non-gradient nonlinearities play a role in the dynamics, there is a region of instability which is not found for the case of $h_1 = h_2 = 0$.

To determine all stability conditions, one must determine the $O(\gamma_1^2)$ and $O(\gamma_2^2)$ corrections to the eigenvalues $\Lambda = 0$. Scaling $\Lambda = O(\gamma_1^2)$ or $\Lambda = O(\gamma_2^2)$ we determine the higher order corrections. For $0 < \gamma_1 = \gamma_2 \ll 1$, the conditions for $\Lambda < 0$ are

$$d + \frac{4d^2q^2 - (h_1 + h_2)^2 r_0^2}{\Lambda_5} > 0,$$

$$\Lambda_4\Lambda_5 d + 4d^2q^2(2br_0^2 - Br_0) + ((2b - 4f)r_0^2 - 3B)(h_1^2 + h_2^2)r_0^2 + 4dq\Lambda_5(h_1 - h_2)r_0 - 2h_1h_2r_0^2(4br_0^2 - 2fr_0^2 - 3Br_0) > 0. \quad (3.9)$$

These conditions are shown in Figure 2. In Figure 2(a), the stability region is shown for $h_1 = h_2 = 0$, the case of Rayleigh–Bénard convection or Swift–Hohenberg-type models. In Figure 2(b), the stability region is shown when non-gradient nonlinearities influence the pattern dynamics.

https://doi.org/10.1017/S095679259800360X Published online by Cambridge University Press

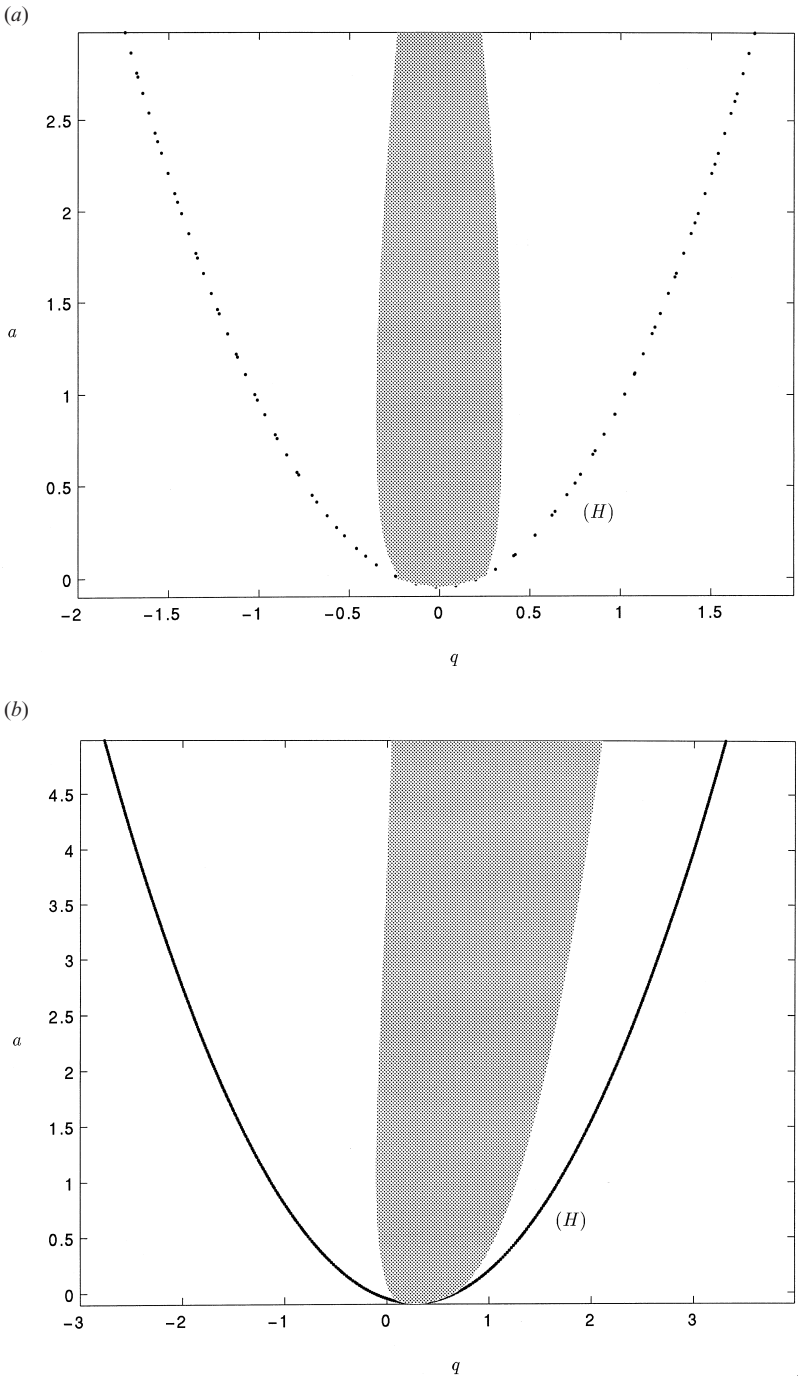


FIGURE 2. Effect of non-gradient terms on the stability of perfect hexagonal patterns for $c = d = 1$, $b = -1$, $f = -2$. Perfect hexagonal patterns exist above the curve (H). (a) For values of q and a in the shaded region and $h_1 = h_2 = 0$, as in Suschik & Tsimring [10], perfect hexagonal patterns are stable to long wave perturbations ($\gamma_1 \ll \gamma_2 \ll 1$ in equation (3.7)). (b) For values of q and a in the shaded region and $h_1 = -1$ and $h_2 = 1$, perfect hexagonal patterns are stable to long wave perturbations ($\gamma_1 \ll \gamma_2 \ll 1$ in equation (3.7)).

https://doi.org/10.1017/S095679259800360X Published online by Cambridge University Press

3.2 Stability of rolls

Some of the numerical computations demonstrate that hexagons may lose their stability to rolls. We therefore consider the stability of rolls in the context of (1.2), i.e. the stability of rolls to hexagonal perturbations. Proceeding as in the previous analysis, we consider perturbations on a roll $A_1 = r_0 e^{iqX_1}$, $A_2 = A_3 = 0$, with solutions of the form

$$\begin{aligned} A_1 &= (r_0 + \hat{p}_1)e^{iqX_1}, \\ A_2 &= \hat{p}_2 e^{iqX_2}, \\ A_3 &= \hat{p}_3 e^{iqX_3}. \end{aligned} \tag{3.10}$$

The roll solutions satisfy $a - q^2 d + br_0^2 = 0$, and exist for

$$\frac{a - q^2 d}{-b} > 0. \tag{3.11}$$

Writing the perturbations as

$$\hat{p}_j = p_j e^{\sigma t + i\gamma_1 X + i\gamma_2 Y}, \tag{3.12}$$

we determine the stability for all γ_1 and γ_2, using the notation

$$\Gamma_1 = \gamma_1, \quad \Gamma_2 = -\frac{1}{2}\gamma_1 + \frac{\sqrt{3}}{2}\gamma_2, \quad \Gamma_3 = -\frac{1}{2}\gamma_1 - \frac{\sqrt{3}}{2}\gamma_2. \tag{3.13}$$

The conditions are

$$\begin{aligned} \frac{a}{3} &> q^2 d, \quad \text{(Eckhaus stability criterion)}, \\ -2A_2 + d(\Gamma_2^2 + \Gamma_3^2) \pm 2qd(\Gamma_3 - \Gamma_2) &> 0, \\ (h_2\Gamma_3 + h_1\Gamma_2 \pm B)(h_1\Gamma_3 + h_2\Gamma_2) \pm B)r_0^2 & \\ +(\pm(A_2 - \Gamma_3^2 d) + 2qd\Gamma_3)(\pm(A_2 - \Gamma_2^2 d) - 2qd\Gamma_2) &> 0, \end{aligned} \tag{3.14}$$

where

$$A_2 = -2(b - f)r_0^2. \tag{3.15}$$

Figure 3 shows the region in the a-q plane for which rolls are stable to hexagonal perturbations. We note that most of this region corresponds to $q < 0$. However, for $q < 0$ rolls are unstable to transverse perturbations, the so–called zigzag instability. As discussed in Section 2, this instability can be observed using the equations (1.5) instead of equation (1.2).

4 Burner-stabilized flames

In this section we consider a three-dimensional model of burner-stabilized flames, in which the flame is treated as a two-dimensional surface. Then, two-dimensional patterns of this surface (see equation (4.15)) can be studied with the methods discussed in §2. The model we employ is a straightforward extension to three dimensions of the two-dimensional models used in Matkowsky & Olagunju [19] and Olangunju & Matkowsky [20], and the details are given in Kuske & Matkowsky [7]. As discussed in Kuske & Matkowsky [7] and

https://doi.org/10.1017/S095679259800360X Published online by Cambridge University Press

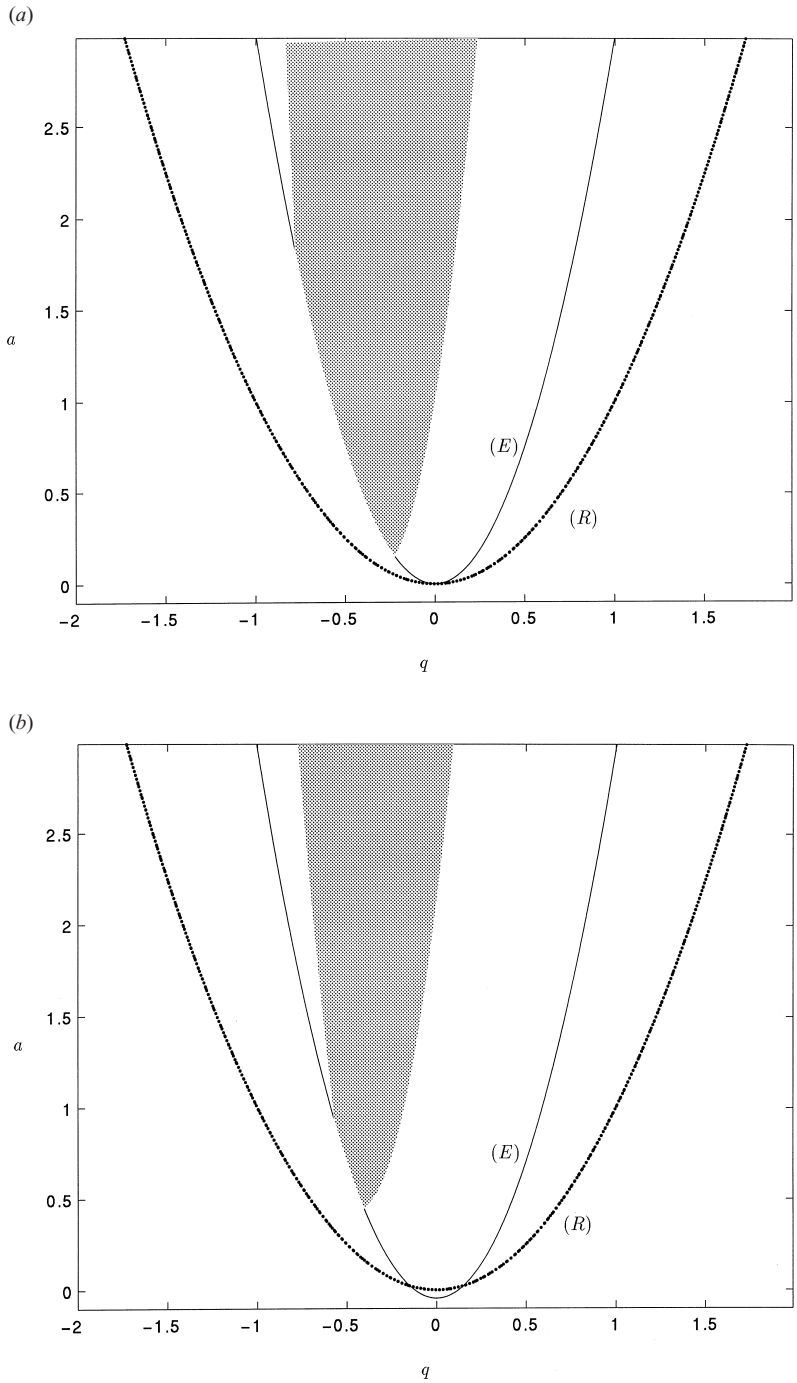


FIGURE 3. Stability of rolls to hexagonal perturbations. (a) Existence and stability of rolls for $c = d = 1$, $b = -1$, $f = -2$, $h_1 = -1$, $h_2 = 1$. Rolls exist above the curve (R). The Eckhaus stability boundary (stability to longitudinal perturbations) is given by (E). In (a) the shaded region corresponds to stability to zero mode perturbations ($\gamma_1 = \gamma_2 = 0$ in (3.12)). In (b) the shaded region corresponds to stability to hexagonal perturbations ($\gamma_1 = \gamma_2 = 0.3$ in equation (3.12).)

https://doi.org/10.1017/S095679259800360X Published online by Cambridge University Press

Olangunju & Matkowsky [20], an analysis based on this model has no restriction on the wavelength of the pattern, in contrast to the analyses of Buckmaster [21] and Shtilman & Sivashinsky [22] which consider only long wavelength instabilities.

We mention a few of the aspects of this model which are pertinent to the following discussion. The burner is modelled as a heat sink [23], with assumptions of weak thermal expansion of the gas and large activation energy. Then the reaction zone is a narrow region of width $O(1/Z)$, where Z is the (non-dimensional) Zeldovich number, which is proportional to the activation energy and typically large in combustion models ($Z > 10$). For large Z, As $Z \to \infty$, this zone can be approximated by a front whose location is given by

$$x_3 = \Phi(t, x_1, x_2). \tag{4.1}$$

We employ non-dimensional cartesian coordinates (x_1, x_2, x_3), with the burner located at $x_3 = 0$. We also assume that there is a single deficient component of the reaction so that only its mass fraction evolves, while the mass fractions of all other components are so abundant that they can be considered to be constant. The reaction–diffusion model is based on perturbations expansions in powers of Z^{-1} of the non-dimensional temperature T and the mass fraction Y of the deficient component. The Lewis number L, which is the ratio of thermal to mass diffusivities, is assumed to be close to unity and the coefficient H describing heat loss to the burner is assumed to be small. Then L and H are scaled as

$$L = 1 + \frac{\lambda}{Z}, \quad H = \frac{K}{Z}. \tag{4.2}$$

Employing a coordinate system which moves with the flame front

$$z = x_3 - \Phi(t, x_1, x_2), \quad x = x_1, \quad y = x_2, \tag{4.3}$$

and seeking solutions of the form

$$\begin{aligned} Y &= Y_0 + \frac{1}{Z} Y_1 + o\left(\frac{1}{Z}\right), \\ T &= \Theta + \frac{1}{Z} T_1 + o\left(\frac{1}{Z}\right), \\ S &\equiv T_1 + Y_1, \end{aligned} \tag{4.4}$$

the model is given by

$$\Theta + Y_0 \equiv 1, \tag{4.5}$$

$$\begin{aligned} \frac{\partial \Theta}{\partial t} + \left(m - \frac{\partial \Phi}{\partial t}\right) \frac{\partial \Theta}{\partial z} &= \Delta \Theta + \left\{1 + \left(\frac{\partial \Phi}{\partial x}\right)^2 + \left(\frac{\partial \Phi}{\partial y}\right)^2\right\}^{1/2} \exp\left(\frac{S}{2}\right) \delta(z), \\ \frac{\partial S}{\partial t} + \left(m - \frac{\partial \Phi}{\partial t}\right) \frac{\partial S}{\partial z} &= \Delta S + \lambda \Delta \Theta - K \Theta \delta(z + \Phi) \end{aligned} \tag{4.6}$$

with boundary conditions

$$\begin{aligned} \Theta \equiv 1 \text{ for } z > 0, \quad \frac{\partial S}{\partial z} &\to 0 \quad \text{as } z \to +\infty \\ \Theta \to 0, \quad S &\to 0 \quad \text{as } z \to -\infty, \\ |\Theta| < \infty, \quad |S| &< \infty \quad \text{as } x, y \to \pm\infty. \end{aligned} \tag{4.7}$$

https://doi.org/10.1017/S095679259800360X Published online by Cambridge University Press

Also, assuming that the reaction goes to completion at the flame front, we set $Y \equiv 0$ behind the flame (for $z > 0$). In equation (4.6), the parameter m is the flow rate of the fuel, and δ is the Dirac delta function. The operator Δ is the Laplacian in the moving coordinate system.

A steady solution of equations (4.6)–(4.7), termed the basic solution, is given by

$$\Theta_0(z) = \begin{cases} 1, & z > 0 \\ e^{mz}, & z < 0, \end{cases} \tag{4.8}$$

$$S_0(z) = \begin{cases} B, & z > 0 \\ B - \lambda m z e^{mz}, & -h < z < 0 \\ B e^{m(z+h)} - \lambda m z e^{mz}, & z < -h, \end{cases}$$

$$\Phi_0 = h, \tag{4.9}$$

where

$$B = 2\ln(m), \qquad h = \frac{1}{m}\ln\left(\frac{-K}{Bm}\right). \tag{4.10}$$

The basic solution (4.8)–(4.9) represents a stationary planar flame located at the standoff distance $x_3 = h$. Since, $Y_1 = 0$ behind the flame, B in equation (4.10) is the $O(1/Z)$ correction to the flame temperature. As shown in Kuske & Matkowsky [7], the standoff distance h in equation (4.10) is a U-shaped function of m, whose minimum approaches zero as K approaches $2/e$. We note that the basic solution becomes unbounded as $m \to 0$. Hence only values of m bounded away from zero are considered. In addition, we consider values of the heat loss parameter $K > 2/e$ [19], in order to avoid flashback ($h < 0$) for certain values of m. The behaviour of this basic solution is discussed further in Matkowsky & Olangunju [19].

To determine the linear stability of the basic solution we introduce perturbations of the form

$$\begin{aligned} \phi &= \Phi - h, \\ w &= \Theta - \Theta_0(z) - \phi\frac{d\Theta_0}{dz}, \\ v &= S - S_0(z) - \phi\frac{dS_0}{dz}. \end{aligned} \tag{4.11}$$

The linear problem for these perturbations is obtained by substituting equation (4.11) into equations (4.6)–(4.7) and linearizing about $\phi = w = v = 0$,

$$\mathscr{L}\begin{pmatrix} w \\ v \end{pmatrix} \equiv \left[\frac{\partial}{\partial t} + m\frac{\partial}{\partial z}\right]\begin{pmatrix} w \\ v \end{pmatrix} - \left(\frac{\partial^2}{\partial z^2} + \frac{\partial^2}{\partial x^2} + \frac{\partial^2}{\partial y^2}\right)\begin{pmatrix} 1 & 0 \\ \lambda & 1 \end{pmatrix}\begin{pmatrix} w \\ v \end{pmatrix} = 0, \tag{4.12}$$

for $z \neq 0, -h$, with jump conditions which are linear in w, v, and ϕ (see Appendix C), which we denote

$$\mathscr{J}\begin{pmatrix} \phi \\ w \\ v \end{pmatrix} = 0 \tag{4.13}$$

https://doi.org/10.1017/S095679259800360X Published online by Cambridge University Press

and boundary conditions

$$\begin{aligned} w \equiv 0 \text{ for } z > 0, \quad \frac{\partial v}{\partial z} \to 0 \quad & \text{as } z \to +\infty, \\ w \to 0, \quad v \to 0 \quad & \text{as } z \to -\infty, \\ |w| < \infty, \quad |v| < \infty \quad & \text{as } x, y \to \pm\infty. \end{aligned} \tag{4.14}$$

In this model, we consider flows in the z-direction only, and allow the domain to extend to infinity in both the x and y directions. Thus, we expect to obtain two dimensional patterns which do not have a preferred orientation in the x–y plane.

We find that equations (4.12)–(4.14) have solutions of the form

$$\begin{pmatrix} w \\ v \\ \phi \end{pmatrix} = Re^{\omega t + ik_1 x + ik_2 y} \begin{pmatrix} W \\ V \\ [W]_0 \end{pmatrix} + \text{c.c.}, \tag{4.15}$$

where $k_1^2 + k_2^2 = k^2$, R is an arbitrary complex constant, and c.c. denotes complex conjugate. The expressions for $W(z)$ and $V(z)$ and the dispersion relation are in Appendix C. For $\Re(\omega) < 0$ (> 0) the basic solution is stable (unstable). The neutral stability boundary corresponding to $\omega = 0$ is shown for selected values of m and $K = 1$ in [7]. This boundary, given explicitly by

$$\lambda = -2 - 8\frac{k^2}{m^2} + \frac{2K\psi e^{-h\psi}}{m(m-\psi)}, \quad \psi^2 = m^2 + 4k^2, \tag{4.16}$$

delineates the region of cellular instability of the basic solution.

For admissible values of the flow rate m, the neutral stability curve has a local maximum at $(\lambda_c, |k| = k_c)$, where $k_c \neq 0$ corresponds to the most rapidly growing mode of the perturbation (4.15). We perform a local analysis in a neighbourhood of the point (λ_c, k_c) seeking stationary non-planar solutions which represent time-independent two-dimensional cellular flames which bifurcate from the basic solution (4.8)–(4.9). We employ an expansion in terms of ϵ, as described in the previous section,

$$\lambda \sim \lambda_c(1 + v\epsilon^2 + \ldots), \tag{4.17}$$

$$w \sim \epsilon w_1 + \epsilon^2 w_2 + \epsilon^3 w_3 + \ldots \tag{4.18}$$

and similarly for v and ϕ. Accordingly, we employ the scaled temporal and spatial variables as in equation (2.11), $T = \epsilon t$, $\tau = \epsilon^2 t$, $\eta = \epsilon x$ and $\zeta = \epsilon y$. The expansion of λ implies that the basic solution $S_0(z)$ is expanded in ϵ as well.

Substituting equations (4.17)–(4.18) into equations (4.5)–(4.7) and equating like powers of ϵ we obtain the sequence of equations

$$\mathscr{L}\begin{pmatrix} w_j \\ v_j \end{pmatrix} = \begin{pmatrix} r_{j1} \\ r_{j2} \end{pmatrix} z \neq 0, -h, \tag{4.19}$$

https://doi.org/10.1017/S095679259800360X Published online by Cambridge University Press

with jump conditions

$$\mathscr{J}\begin{pmatrix}\phi_j\\ w_j\\ v_j\end{pmatrix}=\begin{pmatrix}0\\ \rho_{j0}\\ \rho_{j1}\\ \rho_{j2}\\ \rho_{j3}\\ \rho_{j4}\end{pmatrix} \tag{4.20}$$

and boundary conditions (4.14). To leading order, ($O(\epsilon)$) this yields the linear problem (4.12)-(4.14) with $r_{11}=r_{12}=\rho_{10}=\rho_{11}=\rho_{12}=\rho_{13}=\rho_{14}=0$. Then

$$\begin{pmatrix}w_1\\ v_1\\ \phi_1\end{pmatrix}=(R_1e_1+R_2e_2+R_3e_3+\text{c.c.})\begin{pmatrix}W(z)\\ V(z)\\ 1/m\end{pmatrix},\quad =-\frac{k_c}{2},\quad k_2=\frac{\sqrt{3}k_c}{2}, \tag{4.21}$$

where $W(z)$ and $V(z)$ are given in equations (C)–(C) with λ, k and ω replaced by λ_c, k_c and zero, respectively, and e_1, e_2 and e_3 are as in equation (2.10). Since we perform our analysis in the neighbourhood of the local maximum (λ_c,k_c) of the neutral stability curve, all other modes decay exponentially in time. At this order the complex coefficients $R_n(T,\tau,Y,Z)$ $(n=1,2,3)$ are undetermined.

We proceed as in §2 to determine the amplitude equations for R_n. The non-zero inhomogeneous terms r_{j1}, r_{j2}, ρ_{j0}, ρ_{j1}, ρ_{j2}, ρ_{j3}, ρ_{j4} for $j=1,2,3$ are given in [7] for the case of no spatial modulations (R_j is a function of τ only). Here, there are additional terms from the spatial derivatives.

The solvability condition is applied, as in equation (2.19). In this case it is

$$\left\langle\begin{pmatrix}r_{j1}\\ r_{j2}\end{pmatrix},\begin{pmatrix}w^*\\ v^*\end{pmatrix}\right\rangle=0, \tag{4.22}$$

where the vector $(w^*,v^*)^T$ is the steady solution to the problem adjoint to (4.12)–(4.14) with $\lambda=\lambda_0$. This adjoint solution is given in Kuske & Matkowsky [7].

At $O(\epsilon^2)$, we obtain the solvability condition (2.20) with

$$c_0=\frac{\alpha}{\lambda_c}\left(\frac{5\alpha^3-8m\alpha^2+3m^2\alpha}{4m^2}-\frac{\alpha Ke^{-h\alpha}}{m}+\frac{Ke^{-hp}(-m^2+\alpha^2)}{4m^2}\right). \tag{4.23}$$

The solution for $j=2$ is determined as described in Appendix A, where the coefficients B_n are

$$B_n=\begin{pmatrix}W_{2n}(z)\\ V_{2n}(z)\\ [W_{2n}]_0/m\end{pmatrix}, \tag{4.24}$$

where W_{2n} and V_{2n} for $n=1,2,3,4$ are given in Kuske & Matkowsky [7] and

$$W_{25}=\frac{\partial W}{\partial(k_c^2)},\quad V_{25}=\frac{\partial V}{\partial(k_c^2)}, \tag{4.25}$$

For $j=3$ we apply the solvability condition to obtain the amplitude equations (2.23). The graphs of the coefficients for $K=1$ are given in Figures 4(a) and (b). Accordingly, the stability region for perfect hexagonal patterns on the reaction front is given in Figure 5

https://doi.org/10.1017/S095679259800360X Published online by Cambridge University Press

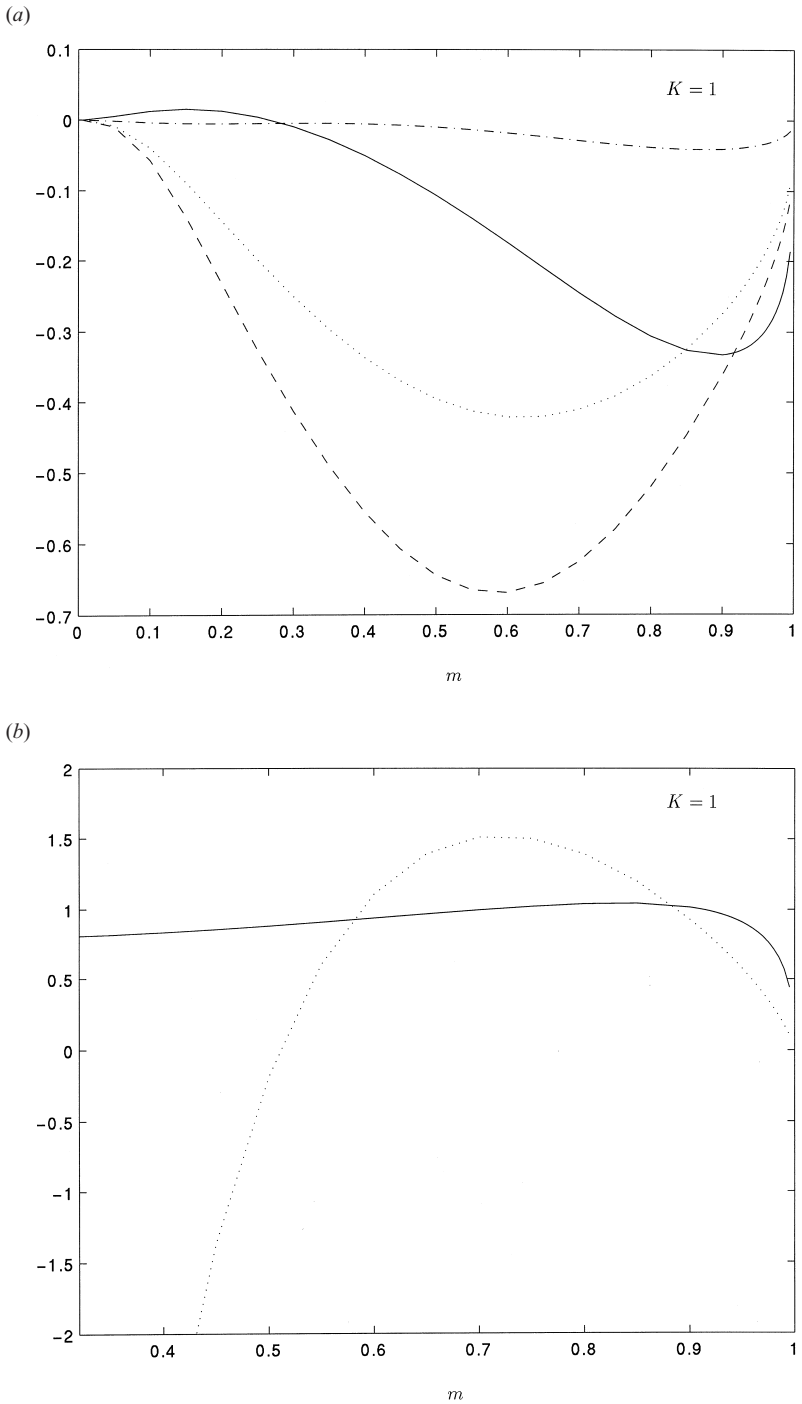


FIGURE 4. (a) The coefficients c (dot-dashed), b (dotted), f (dashed) and h_2 (solid) for $K = 1$ in §4. (b) The coefficients d (solid) and h_1 (dotted) for $K = 1$ in §4.

https://doi.org/10.1017/S095679259800360X Published online by Cambridge University Press

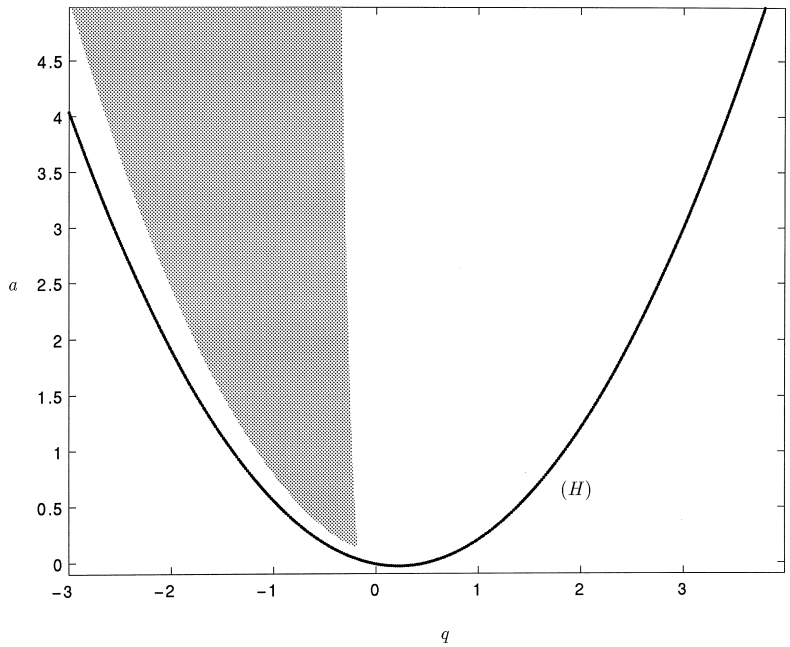


FIGURE 5. Stability region of perfect hexagonal patterns as predicted by the analysis of §3 for the model described in §4 with $m = 0.7$ and $K = 1$, so that $c = -0.28\,7079$ ($c = c_0/\epsilon$, $\epsilon = 0.1$), $b = -0.41\,0856$, $d = 0.994\,014$ $f = -0.625\,134$, $h_1 = 1.509\,53$ and $h_2 = -0.245\,025$. Perfect hexagonal patterns exist above the dotted curve. For values of q and a in the shaded region perfect hexagonal patterns are stable to long wave perturbations ($\gamma_1 \ll \gamma_2 \ll 1$ in equation (3.7)).

for these parameter values. We note that it is necessary to take $c = c_0/\epsilon$ to account for the fact that the terms in the amplitude equation are obtained from two solvability conditions at different orders, as in (2.23).

5 Numerical experiments

In this section we present numerical computations of equations (1.2) and (1.5). These experiments demonstrate the new behaviour described by the evolution equations (1.2) in the general model of §2 and for the application of §4. The method used to solve the amplitude equations is described in detail in §6. In the figures we present the actual pattern u_1 defined in equation (2.9). In doing so, we must choose the critical wavenumber k_c discussed in §2. For a particular application of the form (2.1) one has to calculate this wavenumber. For our purposes we choose an appropriate k_c for the general model and calculate k_c for the model of burner stabilized flames. Since the modulations equations (1.2) and (1.5) govern slow modulations of the rolls, $k_c \gg \epsilon q_{max}$, where q_{max} is the highest Fourier mode resolved by our numerical scheme. This is consistent with the form of equation (2.9), since R_j gives a slowly varying modulation to the pattern with wave number k_c. The figures shown are approximately the size of the computational domain in the X, Y plane (recall that the computational domain is hexagonal). The computations

https://doi.org/10.1017/S095679259800360X Published online by Cambridge University Press

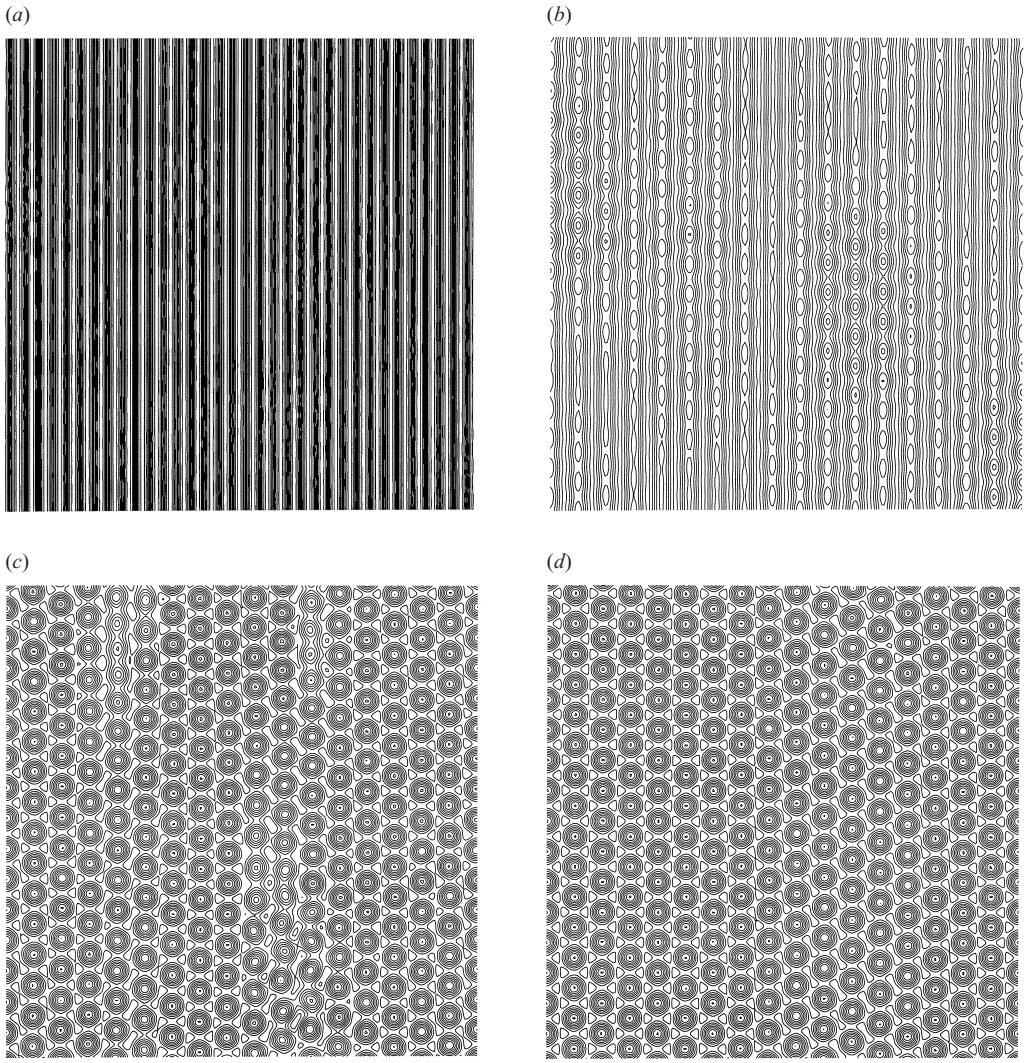


FIGURE 6. Snapshots of the pattern from a computation of equation (1.2) with parameters $a = 1.5$, $c = 1.0$, $b = -1.0$, $d = 1.0$ $f = -2.0$, $h_1 = -1.0$ and $h_2 = 1.0$. The initial data is a roll $q = 0.5$ with a small random perturbation. From the analysis in §3, the roll is unstable (see Figures 3(a) and (b)). The figures show the contours of u_1 in equation (2.9). For the purposes of the figure, we choose $k_c = 8.0$. The final state consists of asymmetric hexagons. The solution is shown at (a) $t = 0$, (b) $t = 2.25$, (c) $t = 30$, (d) $t = 90$.

validate the stability analysis of §4 and demonstrate additional instabilities to asymmetric perturbations occurring for $h_1, h_2 \neq 0$ and parameter ranges for which the pattern is stable to symmetric perturbations.

Figure 6 shows the evolution of equation (1.2) for a case in which the initial rolls would be Eckhaus-stable if $h_1 = h_2 = 0$. According to Figures 3(a) and (b), these rolls are unstable. This is confirmed by the computation, in which the final state consists of

https://doi.org/10.1017/S095679259800360X Published online by Cambridge University Press

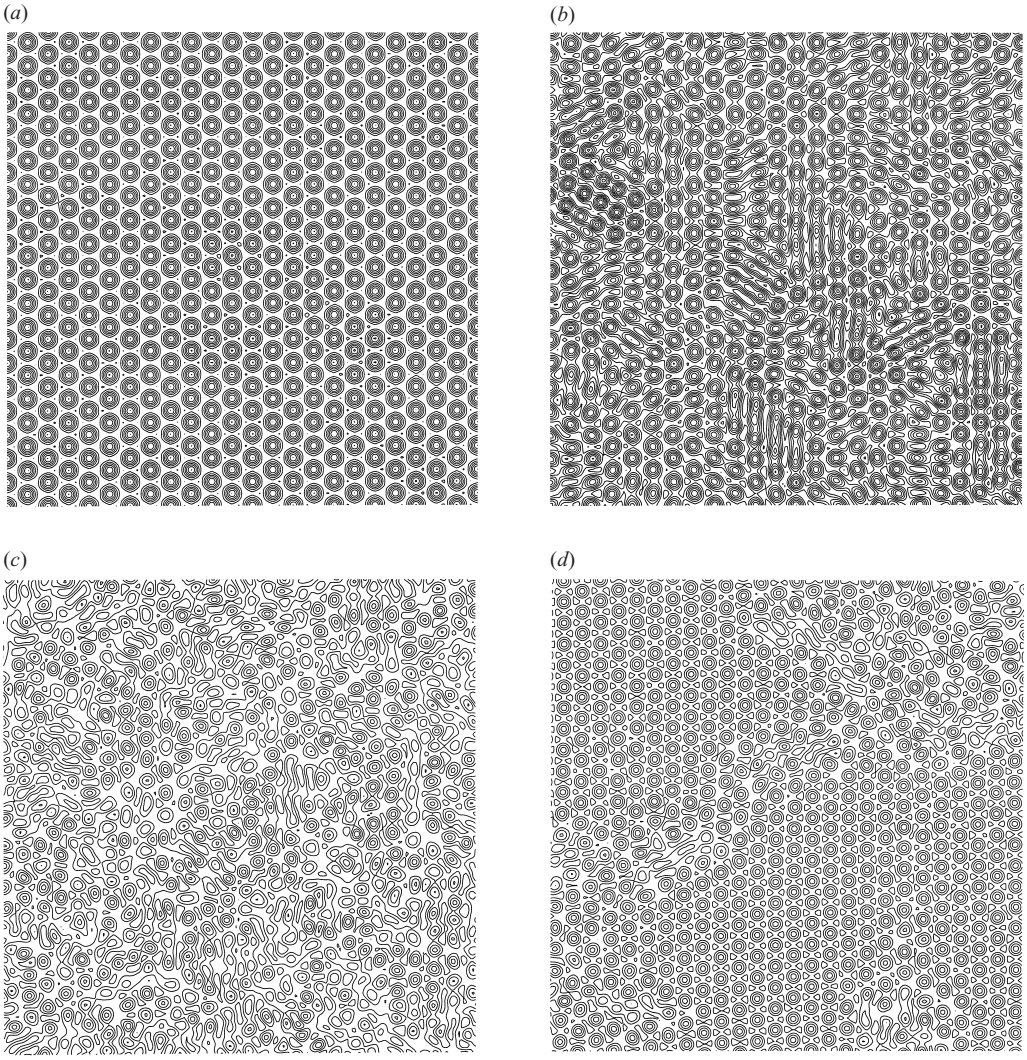


FIGURE 7. Snapshots of the pattern from a computation of equation (1.2) with parameters $a = 2.0$, $c = 1.0$, $b = -1.0$, $d = 1.0$, $f = -2.0$, $h_1 = -1.0$ and $h_2 = 1.0$. The initial data is a perfect hexagon ($q = -0.25$) with a small random perturbation. From the analysis in §3, the hexagon is unstable (see Figure 2). The figures show the contours of u in equation (2.9). For the purposes of the figure, we choose $k_c = 6.0$. The solution is shown at (a) $t = 0$, (b) $t = 6$, (c) $t = 10$, (d) $t = 300$.

asymmetric hexagons, i.e. hexagons of the form (2.9), for which the modulations R_j are not all equal. In the notation of equation (6.5) the final state has most of the energy in $b^1_{2,0}$, $b^2_{4,0}$, $b^3_{3,1}$. Since the fast variation in the figure is due to k_c, this asymmetry is not immediately apparent.

Figure 7 shows the evolution of equation (1.2) for a case where the initial hexagons are unstable according to Figure 1. For $h_1 = h_2 = 0$ such hexagons would be stable. Here the solution does not seem to reach a uniform final state, but a state in which a patch of irregularities coexists with a region hexagons.

https://doi.org/10.1017/S095679259800360X Published online by Cambridge University Press

Figure 8 corresponds to the evolution of equation (1.5) for a roll which is stable according to the calculations performed in Section 3, but with $\epsilon \neq 0$ is zigzag unstable in equation (1.5). The zigzag instability is not apparent since there are other asymmetric perturbations that grow faster. If the run is repeated with $h_1 = h_2 = 0$ then the zigzag instability is observed. The final pattern is composed of perfect hexagons. We have not performed a systematic study of the appearance of asymmetric instabilities as h_1 and h_2 are varied. For certain values of h_1 and h_2 the zigzag instability is still observed.

Figure 9 shows the evolution of equation (1.2) for the model of burner-stabilized flames discussed in §4. The coefficients in the evolution equations are determined for $m = 0.7$ and $K = 1$. This choice of parameters is representative of a range of values of m and K for which the analytical stability results are similar. In this case a perfect hexagonal pattern, which is stable under symmetric perturbations, is perturbed asymmetrically. The pattern is unstable to this perturbation, and Figure 9 shows the evolution to a stable asymmetric hexagonal pattern.

6 Numerical method

Equations (1.2) and (1.5) were solved numerically using spectral differences in space and finite differences in time. The method used differs from previous methods in two important ways, which improve accuracy and speed. Since these improvements are applicable to a large class of problems, we explain them in detail here.

Consider equations (1.2). They are usually written in the form

$$\frac{\partial R_j}{\partial \tau} = \mathscr{L}_j(\partial_X, \partial_Y)R_j + \mathscr{N}_j(R_j, R_k, R_l), \tag{6.1}$$

where permutations of j, k, l yield the three amplitude equations, and repeated indices no longer denote summation. For numerical purposes, the linear operators $\mathscr{L}_j$ may contain any combination of X, Y derivatives, and the nonlinear term $\mathscr{N}$ may also contain terms where R_j, R_k, R_l are differentiated.

In integrating equation (6.1), one is interested in the dynamics of one or a few adjoining hexagons (recall that these equations govern long modulations of some hexagonal solution with wavenumber k_c in equation (2.10)). To simplify the computations, the solution is usually assumed periodic in (X, Y). Then, to minimize the effects of a rectangular domain on solutions with hexagonal structure, one must make the rectangular computational domain large enough so that the central hexagons are unaffected by the boundaries.

To overcome this problem, we choose to solve the equations with the hexagonal symmetry apparent (1.2, 1.5), and assume that the solutions are periodic in (X_1, X_2, X_3). Those equations have the general form

$$\frac{\partial R_j}{\partial \tau} = \mathscr{L}(\partial_{\eta_j}, \partial_{\xi_j})R_j + \mathscr{N}(R_j, R_k, R_l). \tag{6.2}$$

Considering (X_1, X_2, X_3) as independent variables, we can solve equation (6.2) with periodic boundary conditions on (X_1, X_2, X_3) (i.e. solving the equations on the 3-torus). This increases the dimension for the problem by one, but it is easy to show that it does not increase the computational work for a given resolution in the X, Y plane. The method

https://doi.org/10.1017/S095679259800360X Published online by Cambridge University Press

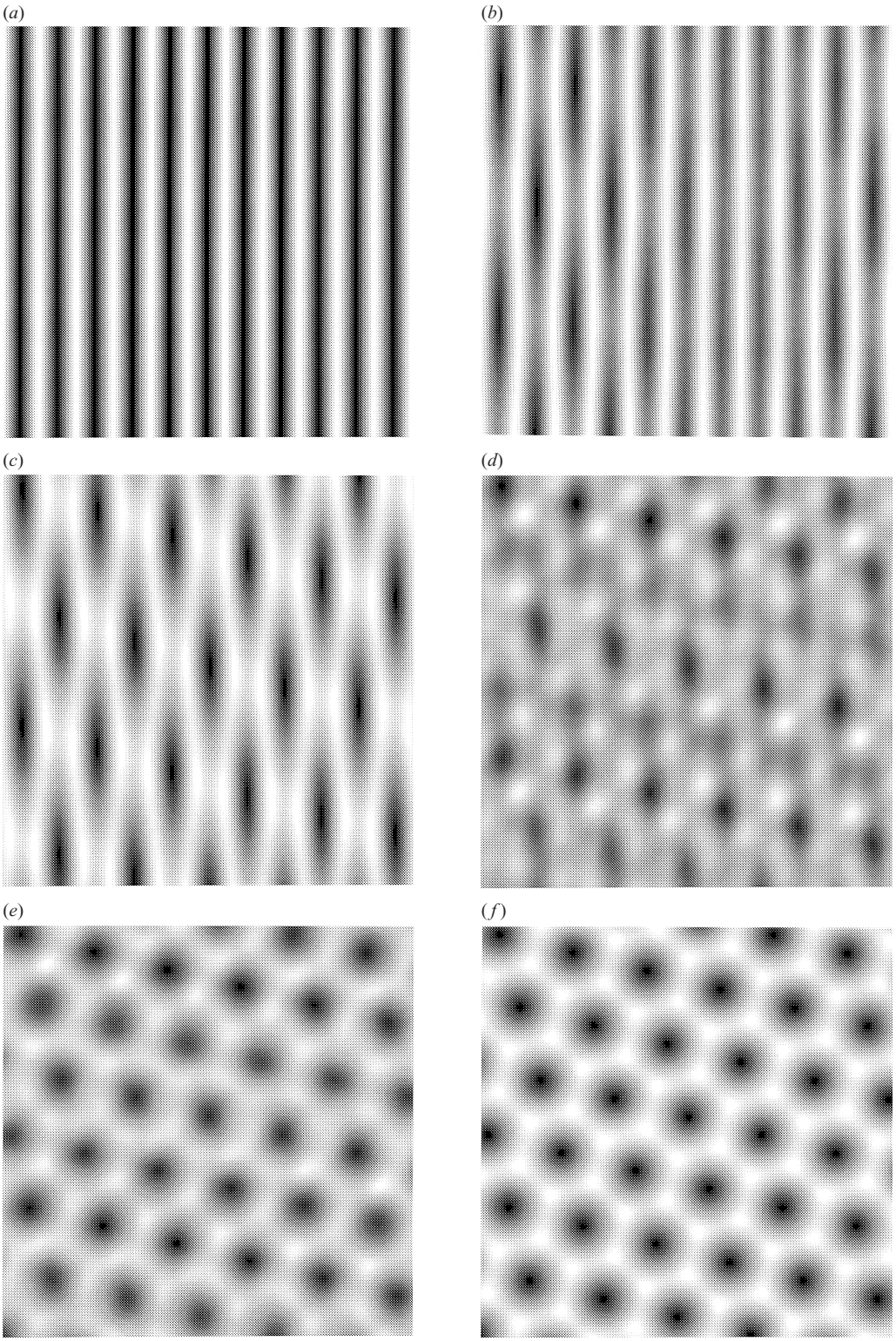


FIGURE 8. For legend see facing page.

https://doi.org/10.1017/S095679259800360X Published online by Cambridge University Press

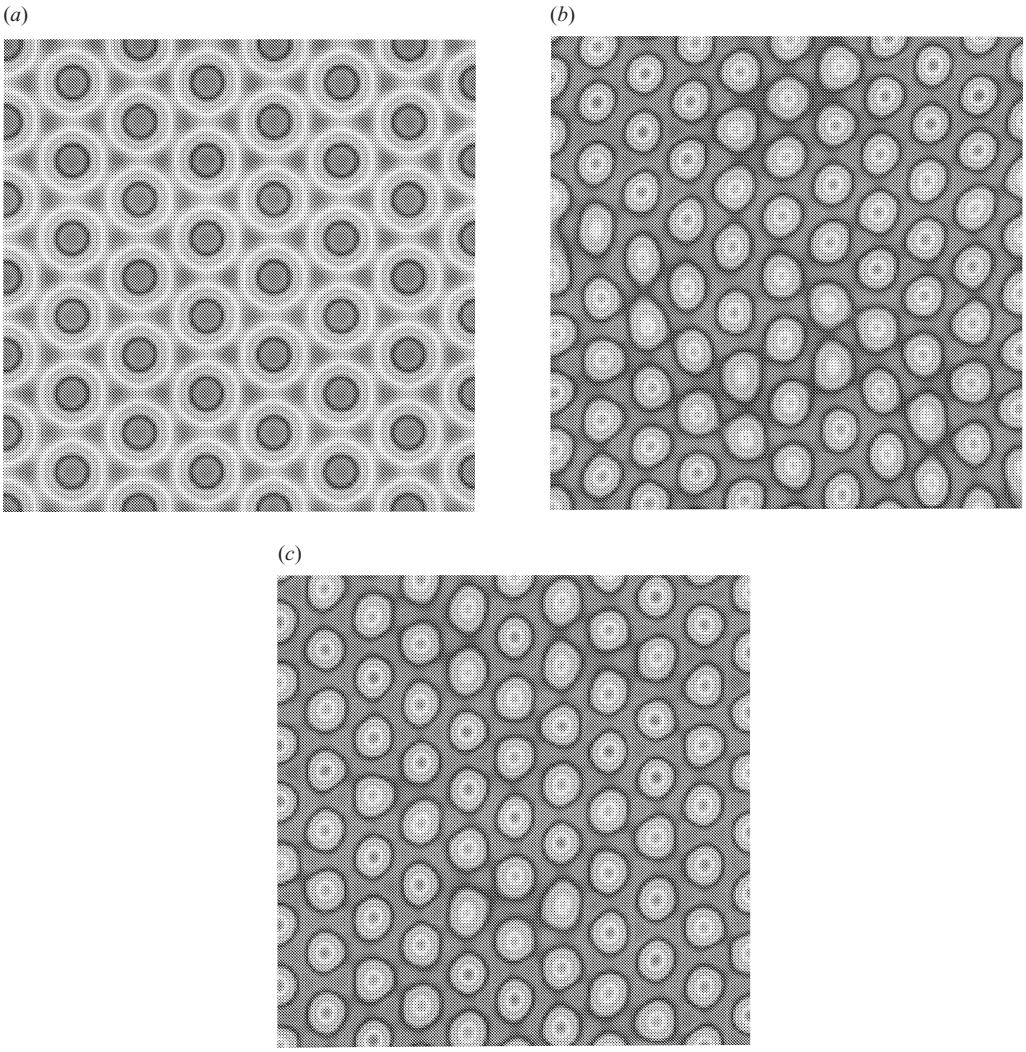


FIGURE 9. Snapshots of the pattern from a computation of equation (1.5) for the combustion model of §4 with parameter values $m = 0.7$ and $K = 1$, so that $k_c \approx 3.9$. The initial pattern, corresponding to $a = 1$ and $q = -0.5$, is stable to hexagonal perturbations, as shown in Figure 5. For sufficiently large asymmetric perturbations, the pattern destabilizes and evolves to an asymmetric hexagonal pattern. The snapshots are at times $t = 0$, $t = 35$ and $t = 250$. The shading variation corresponds to the variation of u_1 in equation (2.9).

FIGURE 8. Snapshots of the pattern from a computation of equation (1.5) with parameters $a = 2.0$, $c = 1.0$, $b = -1.0$, $d = 1.0$, $\epsilon = 1.0$, $f = -2.0$, $h_1 = -1.0$ and $h_2 = 1.0$. The initial data is a zigzag unstable roll $q = -0.5$ with a small random perturbation. The shading variation in the figures shows the variation of u_1 in equation (2.9). For the purposes of the figure, we choose $k_c = 6.0$. The solution is shown at (a) $t = 0$, (b) $t = 3.1$, (c) $t = 6$, (d) $t = 11.45$, (e) $t = 11.6$, (f) $t = 12$.

https://doi.org/10.1017/S095679259800360X Published online by Cambridge University Press

does, nevertheless, preserve the hexagonal symmetry of the problem, and is equivalent to integrating the problem on a hexagonal grid in space. Once a solution in terms of a triple Fourier series for (X_1, X_2, X_3) is computed, we map it back to a double Fourier series in (η_j, ξ_j), to graph and interpret the results. Recall that (η_j, ξ_j) are coordinates parallel and perpendicular to the wave-vectors in equation (2.10), and thus have clear significance as modulations parallel or perpendicular to the rolls. For mode j, and even permutations of j, k, l, we have

$$X_j = \eta_j, \qquad X_k = -\frac{1}{2}\eta_j + \frac{\sqrt{3}}{2}\xi_j, \qquad X_l = -\frac{1}{2}\eta_j - \frac{\sqrt{3}}{2}\xi_j. \tag{6.3}$$

Thus, from a solution in terms of the Fourier decomposition of R_j in (X_1, X_2, X_3) of the form

$$R_j(X_1, X_2, X_3, \tau) = \sum_{l=-N}^{N} \sum_{m=-N}^{N} \sum_{n=-N}^{N} a^j_{lmn}(\tau) \mathrm{e}^{i(lX_1 + mX_2 + nX_3)}, \tag{6.4}$$

we can reconstruct the solution in (η_j, ξ_j) as

$$R_j(\eta_j, \xi_j, \tau) = \sum_{p=-4N}^{4N} \sum_{q=-2N}^{2N} b^j_{pq}(\tau) \mathrm{e}^{i\left(\frac{1}{2}p\eta_j + \frac{\sqrt{3}}{2}q\xi_j\right)}. \tag{6.5}$$

The coefficients $b^j_{pq}(\tau)$ are found in terms of $a^j_{lmn}(\tau)$ by the relation

$$b^j_{pq} = \sum_{l=-N}^{N} a^j_{l, l+\frac{1}{2}(q-p), l-\frac{1}{2}(q+p)}, \tag{6.6}$$

for $q + p$ even and $-N \leqslant l \pm \frac{1}{2}(q \mp p) \leqslant N$, and $b_{pq} = 0$ for $q + p$ odd.

We now briefly describe the method used to compute triply periodic solutions to equation (6.2). We use a method which consists in computing directly the solution of the Fourier transform of equation (6.2), and which computes the linear part of equation (6.2) exactly [24]. For nonlinear problems with stiff linear parts this spectrally accurate method has the advantage of circumventing the stiffness by treating the linear part analytically. By denoting $\mathscr{F}$ the Fourier transform operation from (X_1, X_2, X_3) to the Fourier variables $\mathbf{K} = (K_1, K_2, K_3)$, $\mathscr{F}^{-1}$ its inverse, and $\hat{R}_j(\mathbf{K}, \tau)$ the Fourier transform of R_j, the transform of (6.1) is then

$$\frac{d\hat{R}_j}{d\tau} = \hat{\mathscr{L}}_j \hat{R}_j + \mathscr{F}\{\mathscr{N}\}. \tag{6.7}$$

Here, $\hat{\mathscr{L}}_j(\mathbf{K})$ is the Fourier symbol of $\mathscr{L}$ in (6.2), i.e. for even permutations of j, k, l,

$$\hat{\mathscr{L}}_j(\mathbf{K}) = \mathscr{L}\left(i\left(K_j - \frac{1}{2}(K_k + K_l)\right), \quad i\left(\frac{\sqrt{3}}{2}(K_k - K_l)\right)\right). \tag{6.8}$$

The nonlinear term $\mathscr{N}$ in equation (6.7) is computed in real space. If $\mathscr{N}$ contains terms, where R_j, R_k, R_l are differentiated, these derivatives are first computed in the Fourier domain before computing $\mathscr{N}$.

https://doi.org/10.1017/S095679259800360X Published online by Cambridge University Press

We now use an integrating factor to eliminate the linear part of (6.7). Defining $\hat{R}_j = \hat{S}_j(\mathbf{K}, \tau)\mathrm{e}^{\hat{\mathscr{L}}_j\tau}$, equation (6.7) becomes

$$\frac{d\hat{S}_j}{d\tau} = \mathrm{e}^{-\hat{\mathscr{L}}_j\tau}\mathscr{F}\{\mathscr{N}\}. \tag{6.9}$$

If one considers the initial value problem on a periodic domain (3-torus), and discretizes (X_1, X_2, X_3) with $N \times N \times N$ points, then equation (6.9) becomes a set of N^3 first order, ordinary differential equations for the amplitudes of the Fourier modes. Thus, (6.9) can now be integrated in time with a standard finite difference method such as Runge–Kutta.

The greatest advantage of using equation (6.9), is that the linear part is integrated exactly (clearly, if $\mathscr{N} = 0$, we recover the exact solution to the partial differential equation (6.1)). Thus, this method has no stability restrictions arising from the linear operators in equation (6.1).

7 Conclusion

We have derived new evolution equations for hexagonal patterns in general reaction–diffusion models (1.2). These equations are obtained using a perturbation expansion in which the new non-gradient terms appear at the same order as the usual cubic terms which stabilize the bifurcating hexagonal pattern. We study the new instabilities described by these nonlinearities using both analytical and computational methods. A stability analysis gives the stability criteria for perfect hexagons and rolls, which are confirmed by the computations. Furthermore, we demonstrate computationally that there are other stable patterns composed of both rolls and hexagons. The numerical method is based on the hexagonal structure of the equations, thus removing boundary effects that can arise from a rectangular grid. We have computed these patterns for both a general reaction–diffusion system and a specific model of burner–stabilized flames. These results show a rich variety of modulated two dimensional patterns described by these evolution equations.

Acknowledgements

The authors wish to thank Professor Bernard J. Matkowsky for bringing this problem to their attention.

R. Kuske was supported in part by a NSF Mathematical Sciences Postdoctoral Research Fellowship. P. Milewski was supported in part by NSF Grant DMS 9401405.

Appendix A

The solvability condition obtained at $O(\epsilon^2)$ is

$$\langle r_2, v_0^* \bar{e}_l \rangle = R_{l\,T} - c_0 \overline{R}_m \overline{R}_n = 0, \tag{A 1}$$

Assuming that equation (A 1) is satisfied, u_2 is determined from

$$Lu_2 = u_{1\,T} - \beta_0(u_1, u_1) - 2D(u_{1\,Xx} + u_{1\,Yy}) - \sum_{l=1}^{3} \langle r_2, \bar{e}_l v_0^* \rangle e_l v_0. \tag{A 2}$$

https://doi.org/10.1017/S095679259800360X Published online by Cambridge University Press

The solvability condition obtained at $O(\epsilon^2)$ has been used strategically to add zero to the equation for u_2. It is then straightforward to solve for u_2 from equation (A 2). Substituting equation (2.9) in equation (2.1), we find that

$$\begin{aligned} u_2 = {} & B_1[R_1^2e_1^2 + R_2^2e_2^2 + R_3^2e_3^2 + \text{c.c.}] + B_2[R_1\overline{R}_1 + R_2\overline{R}_2 + R_2\overline{R}_2] \\ & + B_3[R_1\overline{R}_2e_1\bar{e}_2 + R_1\overline{R}_3e_1\bar{e}_3 + R_3\overline{R}_2e_3\bar{e}_2 + \text{c.c.}] \\ & + B_4[\overline{R}_1\overline{R}_2\bar{e}_1\bar{e}_2 + \overline{R}_1\overline{R}_3\bar{e}_1\bar{e}_3 + \overline{R}_3\overline{R}_2\bar{e}_3\bar{e}_2 + \text{c.c.}] \\ & + 2ik_cB_5[R_{1\eta_1}e_1 + R_{2\eta_2}e_2 + R_{3\eta_3}e_3 + \text{c.c.}] \\ & + S_1e_1v_0 + S_2e_2v_0 + S_3e_3v_0 + \text{c.c.}, \end{aligned} \tag{A 3}$$

where we have used the derivative notation of (1.1). The coefficients B_j can be obtained explicitly from the equation (A 2) and we perform this computation in §4 for the combustion application. The expression for u_2 is used in r_3 to obtain the solvability condition (2.22).

Appendix B

The stability of hexagonal modulations (3.1) is obtained from considering the system

$$\rho_\tau = \mathbf{M}\rho, \tag{B 1}$$

where $\rho = [p_1, p_2, p_3, \Omega_1, \Omega_2, \Omega_3]^T$ and $\mathbf{M}$ is

$$\mathbf{M} = \begin{bmatrix} m_{11}(\Gamma_1) & m_{12} & m_{12} & m_{14}(\Gamma_1) & m_{15}(\Gamma_1,\Gamma_2) & m_{15}(\Gamma_1,\Gamma_3) \\ m_{12} & m_{11}(\Gamma_2) & m_{12} & m_{15}(\Gamma_2,\Gamma_1) & m_{14}(\Gamma_2) & m_{15}(\Gamma_2,\Gamma_3) \\ m_{12} & m_{12} & m_{11}(\Gamma_3) & m_{15}(\Gamma_3,\Gamma_1) & m_{15}(\Gamma_3,\Gamma_2) & m_{14}(\Gamma_3) \\ m_{41}(\Gamma_1) & m_{42}(\Gamma_1,\Gamma_2) & m_{42}(\Gamma_1,\Gamma_3) & m_{44}(\Gamma_1) & m_{45} & m_{45} \\ m_{42}(\Gamma_2,\Gamma_1) & m_{41}(\Gamma_2) & m_{42}(\Gamma_2,\Gamma_3) & m_{45} & m_{44}(\Gamma_2) & m_{45} \\ m_{42}(\Gamma_3,\Gamma_1) & m_{42}(\Gamma_3,\Gamma_2) & m_{41}(\Gamma_3) & m_{45} & m_{45} & m_{44}(\Gamma_3) \end{bmatrix}. \tag{B 2}$$

Here we use

$$\Gamma_1 = \gamma_1, \quad \Gamma_2 = -\frac{1}{2}\gamma_1 + \frac{\sqrt{3}}{2}\gamma_2, \quad \Gamma_3 = -\frac{1}{2}\gamma_1 - \frac{\sqrt{3}}{2}\gamma_2, \tag{B 3}$$

and the entries of $\mathbf{M}$ are given by

$$\begin{aligned} m_{11}(\Gamma) &= a + 3br_0^2 + 2fr_0^2 - d\Gamma^2 - q^2, \\ m_{12} &= Br_0 + 2fr_0^2, \\ m_{14}(\Gamma) &= -2ir_0dq\Gamma, \\ m_{15}(\Gamma,\chi) &= ih_2r_0^2\chi + ih_1r_0^2\Gamma, \\ m_{41}(\Gamma) &= 2idq\Gamma/r_0, \\ m_{42}(\Gamma,\chi) &= ih_2\chi + ih_1\Gamma, \\ m_{44}(\Gamma) &= -Br_0 - d\Gamma^2, \\ m_{45} &= -Br_0. \end{aligned} \tag{B 4}$$

For $h_1 = h_2 = 0$ this yields the same stability results as in Suschik & Tsimring [10]. For

https://doi.org/10.1017/S095679259800360X Published online by Cambridge University Press

$h_j \neq 0$, determining the stability results in terms of the coefficients is considerably more tedious than in Suschik & Tsimring [10], since the matrix **M** is full.

Appendix C

Denoting $[f]_a$ the jump in f across $z = a$,

$$[f]_a = f(t, a^+, x, y) - f(t, a^-, x, y), \tag{C 1}$$

the jump conditions at $z = 0, -h$, written generally in equation (4.13), are specifically

$$\phi = \frac{1}{m}[w]_0, \tag{C 2}$$

$$[v]_0 + \beta[w]_0 = 0, \tag{C 3}$$

$$\left[\frac{\partial w}{\partial z}\right]_0 - m[w]_0 + \frac{m}{2}v(t, 0^+, x, y) = 0, \tag{C 4}$$

$$\left[\frac{\partial v}{\partial z}\right]_0 + \beta\left[\frac{\partial w}{\partial z}\right]_0 + \beta m[w]_0 = 0, \tag{C 5}$$

$$[v]_{-h} = 0, \tag{C 6}$$

$$\left[\frac{\partial v}{\partial z}\right]_{-h} - Kw(t, -h, x, y) = 0. \tag{C 7}$$

The basic mode of equations (4.5)–(4.7), for which we study the evolution has components

$$W = \begin{cases} 0, & z > 0, \\ -e^{pz}, & z < 0, \end{cases}$$

$$V = \begin{cases} A_2 e^{lz}, & z > 0, \\ Ce^{lz} + D_1 e^{pz} + D_2 z e^{pz}, & -h < z < 0, \\ Ee^{pz} + D_2 z e^{pz}, & z < -h, \end{cases} \tag{C 8}$$

where

$$p = \frac{1}{2}\left\{m + \sqrt{m^2 + 4\omega + 4k^2}\right\}, \quad l = m - p, \tag{C 9}$$

$$A_2 = \frac{2l}{m}, \quad C = \frac{2l}{m} + \frac{\lambda(l^2 - k^2)}{(p - l)^2},$$

$$D_1 = \lambda + \frac{2l}{m} - C, \quad D_2 = \frac{\lambda(p^2 - k^2)}{p - l}, \quad E = D_1 + Ce^{h(p-l)}. \tag{C 10}$$

The solution (4.15) is non-trivial if and only if the dispersion relation

$$2l(l - p)^2 + \lambda m(l^2 - k^2) + Km(l - p)e^{-h(p-l)} = 0 \tag{C 11}$$

is satisfied.

References

[1] Swift, J. (1984) Convection in a rotating fluid layer. *Contemp. Math.* **28**, 435–448.

[2] Kuznetsov, E. A., Nepomnyashchy, A. A. & Pismen, L. M. (1995) New amplitude equations for Boussinesq convection and nonequilateral hexagonal patterns. *Physica Lett.* A **205**, 261–265.

https://doi.org/10.1017/S095679259800360X Published online by Cambridge University Press

[3] Lauzeral, J., Metens, S. & Walgraef, D. (1993) On the phase dynamics of hexagon patterns. *Europhys. Lett*. **24**, 707–712.
[4] Hohenberg, P. C., Kramer, L. & Riecke, H. (1985) Effects of boundaries on one-dimensional reaction diffusion equation near threshold. *Physica* D **15**, 402–420.
[5] Ouyang, Q. & Swinney, H. L. (1991) Transition from a uniform state to hexagonal and striped Turing patterns. *Nature, Lond*. **352**, 610.
[6] Geddes, J. B., Indik, R. A., Moloney, J. V. & Firth, W. J. (1994) Hexagons and squares in a passive nonlinear-optical system. *Phys. Rev*. A **50**, 3471–3485.
[7] Kuske, R. & Matkowsky, B. J. (1994) On roll, square, and hexagonal cellular flames. *Euro. J. Appl. Math*. **5**, 65–93.
[8] Malomed, B. A., Nepomnyashchy, A. A. & Nuz, A. E. (1994) Nonequilateral hexagonal patterns. *Physica* D **70**, 357–369.
[9] Hoyle, R. Nonlinear phase diffusion equations for the Eckhaus instabilities of hexagons. Preprint.
[10] Suschik, M. N. & Tsimring, L. S. (1994) The Eckhaus instability in hexagonal patterns. *Physica* D **74**, 90–106.
[11] Gunaratne, G. H., Ouyang, Q. & Swinney, H. (1994) Pattern formation in the presence of symmetries. *Physics Rev*. E **50**, 2802–2820.
[12] Golovin, A. A., Nepomnyaschy, A. A. & Pismen, L. M. (1997) Nonlinear evolution and secondary instabilities of Marangoni convection in a liquid-gas system with deformable interface. *J. Fluid Mech*. **341**, 317–341.
[13] Echebarria, B. & Perez-Garcia. C. (1998) Phase instabilities in hexagonal patterns. *Europhys. Lett*. **43**, 35–40.
[14] Nuz, A., Golovin, A. A., Nepomnyaschy, A. A. & Pismen, L. M. (1997) Stability of rolls and hexagonal patterns in non-potential systems. *Physica* D (to be submitted).
[15] Bernoff, A. J., Kuske, R., Matkowsky, B. J. & Volpert, V. (1995) Mean field effects for traveling wave solutions of reaction–diffusion equations. *SIAM J. Appl. Math*. **55**, 485–519.
[16] DeWit, A., Borckmans, P. & Dewel, G. (1993) Turing structures in the presence of gradients. *Inst. Nonequilibr. Struct*. **4**, 247–258.
[17] Hoyle, R. B. (1993) Long wavelength instabilities of square patterns. *Physica* D **67**, 198–223.
[18] Brand, H. R. (1989) Envelope equations near the onset of hexagonal patterns. *Prog. Theor. Phys. Supp*. **99**, 442–449.
[19] Matkowsky, B. J. & Olagunju, D. (1981) Pulsations in a burner stabilized premixed plane flame. *SIAM J. Appl. Math*. **40**, 551–562.
[20] Olagunju, D. & Matkowsky, B. J. (1990) Burner stabilized cellular flames. *SIAM J. Appl. Math*. **48**, 645–664.
[21] Buckmaster, J. D. (1984) Polyhedral flames – an exercise in bimodal bifurcation analysis. *SIAM J. Appl. Math*. **44**, 40–55.
[22] Shtilman, L. & Sivashinsky, G. (1990) On the hexagonal structure of cellular flames. *Can. J. Phys*. **68**, 768–771.
[23] Carrier, G. F., Fendell, F. E. & Bush, W. B. (1978) Stoichiometry and flameholder effects on a one-dimensional flame. *Combust. Sci. Technol*. **18**, 33–46.
[24] Canuto, C., Hussaini, M. Y., Quarteroni, A. & Zang, T. A. (1988) *Spect. Meth. Fluid Mech*. Springer-Verlag.

https://doi.org/10.1017/S095679259800360X Published online by Cambridge University Press